

Measurement of the Rossiter–McLaughlin Effect in the Transiting Exoplanetary System TrES-1*

Norio NARITA,^{1**} Keigo ENYA,² Bun’ei SATO,³ Yasuhiro OHTA,¹
 Joshua N. WINN,⁴ Yasushi SUTO,^{1,8} Atsushi TARUYA,^{1,8} Edwin L. TURNER,⁵
 Wako AOKI,⁶ Motohide TAMURA,⁶ Toru YAMADA,⁶ and Yuzuru YOSHII^{7,8}

¹ Department of Physics, School of Science, The University of Tokyo,
 7-3-1 Hongo, Bunkyo-ku, Tokyo 113-0033
 narita@utap.phys.s.u-tokyo.ac.jp

² Department of Infrared Astrophysics, Institute of Space and Astronautical Science,
 Japan Aerospace Exploration Agency, 3-1-1 Yoshinodai, Sagamihara, Kanagawa 229-8510

³ Okayama Astrophysical Observatory, National Astronomical Observatory of Japan,
 3037-5 Honjo, Kamogata, Asakuchi, Okayama 719-0232

⁴ Department of Physics, and Kavli Institute for Astrophysics and Space Research,
 Massachusetts Institute of Technology, Cambridge, MA 02139, USA

⁵ Princeton University Observatory, Peyton Hall, Princeton, NJ 08544, USA

⁶ National Astronomical Observatory of Japan, 2-21-1 Osawa, Mitaka, Tokyo 181-8588

⁷ Institute of Astronomy, School of Science,
 The University of Tokyo, 2-21-1 Osawa, Mitaka, Tokyo 181-0015
⁸ Research Center for the Early Universe, The University of Tokyo,
 7-3-1 Hongo, Bunkyo-ku, Tokyo 113-0033

(Received 2007 February 27; accepted 2007 April 9)

Abstract

We report a measurement of the Rossiter–McLaughlin effect in the transiting extrasolar planetary system TrES-1, via simultaneous spectroscopic and photometric observations with the Subaru and MAGNUM telescopes. By modeling the radial velocity anomaly that was observed during a transit, we determine the sky-projected angle between the stellar spin axis and the planetary orbital axis to be $\lambda = 30 \pm 21$ [deg]. This is the third case for which λ has been measured in a transiting exoplanetary system, and the first demonstration that such measurements are possible for relatively faint host stars ($V \sim 12$, as compared to $V \sim 8$ for the other systems). We also derive a time of mid-transit, constraints on the eccentricity of the TrES-1b orbit ($e = 0.048 \pm 0.025$), and upper limits on the mass of the Trojan companions ($\lesssim 14 M_{\oplus}$) at the 3σ level.

Key words: stars: planetary systems: individual (TrES-1) — stars: rotation — techniques: photometric — techniques: radial velocities — techniques: spectroscopic

1. Introduction

The Rossiter–McLaughlin effect (hereafter the RM effect) is a phenomenon originally reported as a “rotational effect” in eclipsing binary systems by Rossiter (1924) (for the Beta Lyrae system) and McLaughlin (1924) (for the Algol system). In the context of extrasolar planetary science, the RM effect is seen as a radial velocity anomaly during a planetary transit caused by the partial occultation of the rotating stellar disk (see Ohta et al. 2005, Giménez 2006, or Gaudi & Winn 2007, for theoretical descriptions). The radial velocity anomaly depends on the trajectory of the planet across the disk of the host star, and in particular on the alignment between that trajectory and the rotation field of the star. By monitoring this anomaly throughout a transit one can determine whether or not the planetary orbital axis is well-aligned with the stellar spin axis. In the Solar System, the orbits of all 8 planets are known to be well-aligned with the solar equator, but this is not necessarily the case for exoplanetary systems, or for hot Jupiters in particular. The key parameter is the sky-projected angle between the stellar spin axis and the planetary orbital axis, λ , and measurements of this “misalignment angle” for various exoplanetary systems will help to place the Solar System in a broader context.

Specifically, measurements of the RM effect for exoplanetary systems are important because of the implications for

* Based in part on data collected at Subaru Telescope, which is operated by the National Astronomical Observatory of Japan.
 ** JSPS Fellow.

theories of migration and hot Jupiter formation. So far, measurements of λ for two systems have been reported; Queloz et al. (2000) and Winn et al. (2005) for HD 209458, Winn et al. (2006c) for HD 189733. In both of those systems, the host star is very bright ($V \sim 8$), facilitating the measurement. The observed values of λ for the two systems are small or consistent with zero, which would imply that the standard migration mechanism (planet-disk interaction) does not alter the spin-orbit alignment grossly during the planetary formation epoch. However, just these few examples are not enough for statistical constraints on other hot Jupiter formation theories, including planet-planet interaction (Rasio & Ford 1996; Weidenschilling & Marzari 1996), the “jumping Jupiter” model (Marzari & Weidenschilling 2002), or the Kozai mechanism (Wu & Murray 2003), which may lead hot Jupiters to have significantly misaligned orbits. Thus further measurements of the RM effect for other transiting systems are valuable. Given that most of ongoing transit surveys target relatively faint ($V \sim 12$) host stars, it is also important to extend the reach of this technique to fainter stars. Further observations for new targets would be useful to constrain planet formation theories, and more importantly, have a potential to discover large spin-orbit misalignments, which would be a challenge to some theoretical models.

In this paper, we report the measurement of the RM effect and the constraint on λ for TrES-1 ($V = 11.8$) which has a significantly fainter host star than those in previous studies ($V \sim 8$). In addition to the fainter host star, this work differs from previous studies of the RM effect in that we have conducted simultaneous spectroscopic and photometric observations. This new strategy offers several potentially important advantages. First, the simultaneous photometry eliminates any uncertainty in the results due to the orbital ephemeris and the transit depth. Although this did not turn out to be crucial for the present work, it will be useful for newly discovered targets which still have uncertainty in the times of transits. Second, the transit depth might be expected to vary due to star spots or transient events, and indeed evidence for star spots was reported in HST/ACS photometry for this system (Charbonneau et al. 2007). Thus simultaneous monitoring is useful to assess anomalies in the transit depth. Finally, obtaining all of the data on a single night is useful to avoid systematic errors in radial velocities from long-term instrumental instabilities. Moreover, although it need not be simultaneous, the photometry also helps to determine the limb-darkening parameter for the visual band, which can be used in the interpretation of the RM-affected spectra.¹ In this way, we can determine the limb-darkening parameter of the host star directly from the data, instead of assuming a value based on stellar atmosphere models.

We describe our observations in Section 2 and report the results in Section 3. Section 4 provides a discussion and summary of this paper.

2. Observations and Data Reduction

We observed the planet-hosting K0V star TrES-1 on UT 2006 June 21, the night of a predicted planetary transit, using the Subaru 8.2 m Telescope at Mauna Kea and the MAGNUM 2 m Telescope at Haleakala, both in Hawaii. The event is predicted as the 238th transit from the first discovery, namely $E = 238$ (E : integer) in the ephemeris by Alonso et al. (2004);

$$T_c(E) = 2453186.8060(\pm 0.0002) + E \times 3.030065(\pm 0.000008) \text{ [HJD].} \quad (1)$$

The transit occurred shortly after midnight. We observed TrES-1 during 5 hours bracketing the predicted transit time, through air masses ranging from 1.0 to 1.3.

2.1. MAGNUM Photometry

The MAGNUM 2 m telescope is located near the Haleakala summit on the Hawaiian Island of Maui (Kobayashi et al. 1998; Yoshii 2002; Yoshii et al. 2003). The MAGNUM photometric observation was conducted in parallel with the Subaru spectroscopic observation. We employed the Multi-color Imaging Photometer (MIP) using a 1024×1024 pixel CCD with a V band filter, covering $4750 \text{ \AA} < \lambda < 6180 \text{ \AA}$, and we set 9 dithering positions (3×3 positions) on the CCD. The MIP has a $1.5 \times 1.5 \text{ arcmin}^2$ field of view (FOV) with a pixel scale of $0.277 \text{ arcsec/pixel}$. We used 2MASS J19041058+3638409 as our comparison star for differential photometry. This star is close enough to fit in the MIP field of view, and is known to be photometrically stable at a level sufficient for our study (e.g., Charbonneau et al. 2005). The exposure time was either 40 or 60 seconds² according to observing conditions, with a readout/setup time of 60 seconds.

We then reduced the images with the standard MIP pipeline described in Minezaki et al. (2004). We determined the

¹ Here we assume that the limb-darkening parameters for the spectroscopic and photometric models are the same. This is likely to be a good approximation because the photometric band is a good match to the region of the optical spectrum where the line centroids are measured (i.e., the region with abundant I_2 absorption lines). However, in principle the correspondence is not exact because the limb-darkening function may not be identical in the lines as opposed to the continuum, and because the influence of the limb darkening function on the RV-measuring algorithm has yet to be investigated in detail.

² We selected the exposure time of our photometric observations so that the photon counts are close to the saturation level of the CCD. Therefore the resulting Poisson uncertainties are almost constant through our observations.

apparent magnitudes of TrES-1 and the comparison star using an aperture radius of 20 pixels. The typical FWHM of each star ranged from 1.4 to 1.9 arcsec (from 5 to 7 pixels). We estimated the sky background level with an annulus from 20 to 25 pixels in radius centered on each star, and subtracted the estimated sky contribution from the aperture flux. Then we computed the differential magnitude between TrES-1 and the comparison star. After these steps, we decorrelated the differential magnitude from the dithering positions and eliminated apparent outliers from the light curve, most of which were obtained at the 9th dithering position. We do not find any clear correlations with other observing parameters.

For the analysis of transit photometry, Pont et al. (2006) studied the time-correlated noise (the so-called “red noise”) in detail, and Gillon et al. (2006) introduced a simple and useful method to account at least approximately for the effect of the red noise on parameter estimation. Based on these studies, we used the following procedure to determine the appropriate data weights for the MAGNUM photometry (which are similar to that employed by Winn et al. 2006a).

We first fitted the MAGNUM light curve with the analytic formula given in Ohta et al. (2005) and found the residuals between the data and the best-fitting model. Using only the Poisson noise as an estimate of the error in each photometric sample, we found $\chi^2/\nu_{dof} \sim 2.8$ (ν_{dof} : degrees of freedom), implying that the true errors are significantly in excess of the Poisson noise. We also found the residuals in the early part of the night (before ~ 2453907.91 [HJD]) to be significantly larger than those from later in the night. This larger scatter could have been caused by shaking of the telescope by the stronger winds that occurred during the early part of the night. We thus estimated error-bars separately for the early part of the night and the later part of the night, as described below.

First, we rescaled the error bars to satisfy $\chi^2/\nu_{dof} = 1.0$ (step 1), namely 0.00259 for the early data and 0.00189 for the late data. The light curve with these rescaled error bars is shown in the upper panel of Fig. 1. Next, in order to assess the size of time-correlated noise for the MAGNUM data, we solved the following equations,

$$\sigma_1^2 = \sigma_w^2 + \sigma_r^2, \quad (2)$$

$$\sigma_N^2 = \frac{\sigma_w^2}{N} + \sigma_r^2, \quad (3)$$

where σ_1 is the standard deviation of each residual and σ_N is the standard deviation of the average of the successive N points. σ_w is called the white noise, which is uncorrelated noise that averages down as $(1/N)^{1/2}$, while σ_r is called the red noise, which represents correlated noise that remains constant for specified N . We calculated σ_w and σ_r for the choice $N = 30$ (corresponding to one hour), finding $\sigma_w = 0.00219$ and $\sigma_r = 0.00139$ for the early data. On the other hand, we found $\sigma_r^2 < 0$ (suggesting a smaller level of the red noise) for the late data. The choice of $N = 30$ is fairly arbitrary; other choices of N between 5 and 50 gave similar results. We then adjusted the error bars for the early night by multiplying $[1 + N(\sigma_r/\sigma_w)^2]^{1/2} \sim 3.6$ (step 2). We did not change the error bars for the late night data. We adopted these rescaled uncertainties for subsequent fitting procedures.

2.2. Subaru HDS Spectroscopy

We used the High Dispersion Spectrograph (HDS) on the Subaru Telescope (Noguchi et al. 2002). We employed the standard I2a set-up of the HDS, covering $4940 \text{ \AA} < \lambda < 6180 \text{ \AA}$ with the Iodine absorption cell for measuring radial velocities. The slit width of $0.^{\prime\prime}8$ yielded a spectral resolution of ~ 45000 , and the seeing was between $0.^{\prime\prime}75$ and $1.^{\prime\prime}2$. The exposure time for TrES-1 was 15 minutes yielding a typical signal-to-noise ratio (SNR) ~ 60 per pixel. In order to estimate systematic errors from short term instrumental variations, we also obtained spectra of the much brighter ($V = 4.7$) K0V star HD 185144 before and after the series of TrES-1 exposures. This star is known to be stable in velocity (Johnson et al. 2006). We obtained five 30 s exposures of HD 185144, each having a SNR of approximately 200 pixel^{-1} .

We processed the frames with standard IRAF³ procedures and extracted one-dimensional spectra. Next, we calculated relative radial velocity variations by the algorithm following Sato et al. (2002). We used this algorithm because it properly takes into account the fairly large changes of the instrumental profile during the observations. The HDS is known to experience appreciable instrumental variations even within a single night⁴. We estimated internal errors of the radial velocities from the scatter of the radial velocity solutions for 2\AA segments of the spectra. The typical errors are $10 \sim 15 \text{ [m s}^{-1}\text{]}$, which are reasonable values to be expected from the photon noise limit. Note that we do not find any evidence of star spots or transient events during our photometric observation (see Fig. 1). For this reason, we have not accounted for possible systematic errors in the velocities due to star spots. We also reduced the HD 185144 spectra with the same method in order to check for systematic errors due to short-term instrumental instabilities. The rms of the radial velocity of HD 185144 is less than 5 m s^{-1} , attesting to good instrumental stability. The resultant radial velocities of TrES-1 and their errors are shown in Table 1 and the lower panel of Fig. 1.

³ The Image Reduction and Analysis Facility (IRAF) is distributed by the U.S. National Optical Astronomy Observatories, which are operated by the Association of Universities for Research in Astronomy, Inc., under cooperative agreement with the National Science Foundation.

⁴ Such variations were reported in Winn et al. (2004) and Narita et al. (2005).

3. Results

As described above, we have obtained 20 radial velocity samples and 184 V band photometric samples taken simultaneously covering the transit. In addition, in order to search for an optimal solution of orbital parameters for TrES-1, we incorporate our new data with 12 previously published radial velocity measurements using the Keck I telescope (7 by Alonso et al. 2004 and 5 by Laughlin et al. 2005) and 1149 z band photometric measurements spanning 3 transits using the FLWO 1.2m telescope (Winn et al. 2006b).⁵ We employ the analytic formulas of radial velocity and photometry including the RM effect given in Ohta et al. (2005) and Ohta et al. (2006) (hereafter the OTS formulae) in order to model the observed data. Here we assume circular orbits of the star and the planet about the center of mass (namely, $e = 0$). We adopt the stellar mass $M_s = 0.87(\pm 0.03)$ [M_\odot] (Laughlin et al. 2005) and the orbital period $P = 3.0300737$ [days] and $T_c(0) = 2453186.80603$ [HJD] (Winn et al. 2006b). As a result, our model has 15 free parameters in total. Eight parameters for the TrES-1 system include the radial velocity amplitude K , the sky-projected stellar rotational velocity⁶ $V \sin I_s$, the misalignment angle between the stellar spin and the planetary orbit axes λ , the linear limb-darkening parameter for V band u_V , the same for z band u_z , the ratio of star-planet radii R_p/R_s , the stellar radius R_s , and the orbital inclination i . We also add three parameters for velocity offsets to the respective radial velocity dataset v_1 (for our template spectrum), v_2 (for Alonso et al. 2004) and v_3 (for Laughlin et al. 2005), and four parameters for the times of mid-transit $T_c(E)$ ($E = 234, 235, 236, 238$).

In previous studies of the exoplanetary RM effect, it was possible and desirable to determine both $V \sin I_s$ and λ from the radial velocity data. In this case, there are two reasons to prefer an external determination of $V \sin I_s$. First, the signal-to-noise ratio of the anomaly is smaller, because of the faintness of the host star. This makes it valuable to reduce the number of degrees of freedom in the model. Second, the transit geometry is nearly equatorial, which introduces a very strong degeneracy between $V \sin I_s$ and λ , as explained by Gaudi & Winn (2007). The alternative we have chosen is to adopt a value for $V \sin I_s$ based on previous observations, and use the radial-velocity anomaly to determine λ . (We have also investigated our ability to determine both parameters, as described below.) Laughlin et al. (2005) reported $V \sin I_s = 1.08 \pm 0.30$ [km s^{-1}] for the TrES-1 host star from their analysis of the observed spectral line profiles; this is the most reliable estimate for $V \sin I_s$ to date. We incorporate this information into our model by adding a term $\left[\frac{V \sin I_s - 1.08}{0.30}\right]^2$ to the χ^2 fitting statistic. Thus our χ^2 statistic is

$$\chi^2 = \sum_{i=1}^{N_{rv}=32} \left[\frac{v_{i,obs} - v_{i,calc}}{\sigma_i} \right]^2 + \sum_{j=1}^{N_f=1333} \left[\frac{f_{j,obs} - f_{j,calc}}{\sigma_j} \right]^2 + \left[\frac{V \sin I_s - 1.08}{0.30} \right]^2, \quad (4)$$

where v_{calc} and f_{calc} represent the values calculated by the OTS formulae with the above parameters. We find optimal parameters by minimizing the χ^2 statistic of Eq. (4) using the AMOEBA algorithm (Press et al. 1992), and estimate confidence levels of the parameters using $\Delta\chi^2$ from the optimal parameter set. To assess the dependence of our results on the *a priori* constraint on $V \sin I_s$, we also compute and compare the best-fit values and uncertainties by using another function:

$$\chi^2 = \sum_{i=1}^{N_{rv}=32} \left[\frac{v_{i,obs} - v_{i,calc}}{\sigma_i} \right]^2 + \sum_{j=1}^{N_f=1333} \left[\frac{f_{j,obs} - f_{j,calc}}{\sigma_j} \right]^2, \quad (5)$$

for reference. In addition, we note that the third radial velocity sample of our data ($t = 2453907.89262$ [HJD]) may appear to be an outlier, but it lies just about 3σ from a theoretical radial velocity curve (e.g., Fig. 2). For clarity, we calculate Eq. (4) and Eq. (5) with and without that sample.

The results for both χ^2 statistics are presented in Table 2. The minimum χ^2 is 1308.57 (1296.39) for Eq. (4) and 1305.18 (1298.57) for Eq. (5) with 1350 (1349) degrees of freedom, where the numbers in parentheses refer to the case without the outlier. In Fig. 2, we present the radial velocities and the best-fit curve with (the top figure, marked with “a”) and without (the middle figure, marked with “b”) the *a priori* constraint. In addition, we also compute the best-fit curve without the constraint, but assuming that $\lambda = 0$ [deg] (the bottom figure, marked with “ $\lambda = 0$ [deg]”). Fig. 3 plots ($V \sin I_s, \lambda$) contours calculated with (the left panel, marked with “a”) and without (the right panel, marked with “b”) the *a priori* constraint.⁷ As a result, we find $\lambda = 30 \pm 21(24 \pm 23)$ [deg] and $V \sin I_s = 1.3 \pm 0.3(1.3 \pm 0.3)$ [km s^{-1}] for TrES-1 with the *a priori* constraint, and our findings except for λ are in good agreement with previous

⁵ The uncertainties of the FLWO data had already been rescaled by the authors such that $\chi^2/\nu_{dof} = 1.0$ for each transit (namely, the step 1 has been done). For the step 2, we find $\sigma_i^2 < 0$ for these data, thus we did not modify these error bars further.

⁶ Based on the previous studies by Winn et al. (2005) and Winn et al. (2006c), we have learned the OTS formulae systematically underestimate the amplitude of radial velocity anomaly by approximately 10%. This is possibly because the radial velocity anomaly defined by Ohta et al. (2005) and that measured by the analysis pipeline are different. Thus we correct $V \sin I_s$ in the OTS formulas by modifying $V \sin I_s(\text{OTS}) = V \sin I_s(\text{real}) * 1.1$. This correction presumably gives more realistic values for $V \sin I_s$ and λ , and has little influence on any of the other parameters.

⁷ We only show here the results with the possible outlier in Fig. 2 and Fig. 3, since the same figures but without the outlier have basically similar appearance and have less information to show.

studies (Alonso et al. 2004; Laughlin et al. 2005; Winn et al. 2006b). On the other hand, the result without the *a priori* constraint, $\lambda = 48 \pm 17 (39 \pm 21)$ [deg] and $V \sin I_s = 2.5 \pm 0.8 (2.1 \pm 0.8)$ [km s $^{-1}$], agrees with the above result within about 1σ for λ and $V \sin I_s$, and is also consistent with the previous results for other parameters. In case we calculate χ^2 without the constraint but assuming that $\lambda = 0$ [deg], we find that the minimum χ^2 is 1309.85 (1298.91) with 1351 (1350) degrees of freedom, and $V \sin I_s = 1.5 \pm 0.5 (1.5 \pm 0.5)$ [km s $^{-1}$]. Consequently, our results for λ have fairly large uncertainties. We find at least that the orbital motion of TrES-1b is prograde. Additional radial velocity measurements during transits, and a more precise measurement of $V \sin I_s$, would be desirable to pin down λ and help to discriminate between different modes of migration.

4. Discussion and Summary

We have presented simultaneous spectroscopy and photometry of a transit of TrES-1b, exhibiting a clear detection of the Rossiter–McLaughlin effect and consequent constraints on the alignment angle between the stellar spin and the planetary orbital axes. Our philosophy has been to use all of the best data available at present. However, it is also interesting to examine how well we are able to determine the system parameters using *only* the data gathered on a single night using Subaru and MAGNUM. This is because for future studies of newly discovered transiting exoplanetary systems, higher-precision data from other observatories may not be available. We repeat the fitting procedure without the Keck and FLWO data but still assuming the system parameters other than $V \sin I_s$, λ , u_V , v_1 , and $T_c(238)$ to be the values presented in Alonso et al. (2004) and Winn et al. (2006b). We find almost the same values and uncertainties for the parameters above (the right side of Table 2) as before, indicating that a single night’s data would have done almost as well as the full data set.

Using transit timing of the TrES-1 system, Steffen & Agol (2005) reported a constraint on the existence of additional planets in the system. Subsequently, Winn et al. (2006b) pointed out that $T_c(E)$ ($E = 234, 235, 236$) are consistent with their ephemeris at about the 2σ level, but occurred progressively later than expected. Here we present $T_c(E)$ ($E = 238$) in Fig. 4. Our result is also consistent with the published ephemeris within 1.5σ , occurring only slightly later than expected from Winn et al. (2006b).

In addition to producing transit timing variations, any additional bodies in the TrES-1 system could excite the orbital eccentricity of the TrES-1b planet, which could be detectable in the radial velocity measurements of the host star. Thus it is worthwhile to put empirical constraints on the orbital eccentricity. For this purpose, we compute χ^2 using Eq. (4) for fixed values of (e, ω) over numbers of grid points to map out the allowed region in (e, ω) space. In fact the most appropriate parameters are $e \cos \omega$ and $e \sin \omega$ since their uncertainties are uncorrelated (see Fig. 5). The resulting constraints are $e \cos \omega = 0.005 \pm 0.005$ and $e \sin \omega = -0.048 \pm 0.024$. Our result for $e \cos \omega$ is similar to that of Charbonneau et al. (2005), which was based on the timing of the secondary eclipse. The value of $e \cos \omega$ is consistent with zero within 1σ , and the value of $e \sin \omega$ is consistent with zero within 2σ . Thus we do not find any strong evidence for a nonzero orbital eccentricity in the TrES-1 system.

There is another interesting application of our data. Recently, Ford & Gaudi (2006) studied the detectability of “hot Trojan” companions near the L4/L5 points of transiting hot Jupiters, through any observed difference between the time of vanishing stellar radial velocity variation (T_0) and the time of the midpoint of the photometric transit (T_c). Our strategy of simultaneous spectroscopic and photometric transit observations is ideally suited for searching for the hot Trojan companions. For the TrES-1 system, Ford & Gaudi (2006) set an upper limit on the mass of the Trojan companions $\simeq 51 M_\odot$ at the 3σ level (assuming the circular orbit), using the radial velocity samples of Alonso et al. (2004). Here we compute $\Delta t = T_0 - T_c(238)$ using all available out-of-transit radial velocity samples with (without) the possible outlier, and both for the circular and the eccentric orbit. We find $\Delta t = 3.2 \pm 11.2 (3.2 \pm 11.8)$ [min] (circular) and $\Delta t = 33.0 \pm 52.6 (33.7 \pm 44.8)$ [min] (eccentric). Accordingly, we set constraints on the mass of the Trojan companions, M_T ⁸, through the relation;

$$M_T \simeq \frac{4\pi}{\sqrt{3}} M_p \frac{\Delta t}{P}, \quad (6)$$

$$\sigma_{M_T} \simeq \frac{4\pi}{\sqrt{3}} M_p \frac{\sigma_{\Delta t}}{P}, \quad (7)$$

where σ_{M_T} and $\sigma_{\Delta t}$ indicate the uncertainties of M_T and Δt , respectively (Eq. (1) and Eq. (2) in Ford & Gaudi 2006). Note that we adopt $M_p = 0.73 \pm 0.03$ which are determined by this work. We find $M_T = 1.2 \pm 4.3 (1.2 \pm 4.6)$ [M_\oplus] (circular) and $M_T = 13 \pm 20 (13 \pm 17)$ [M_\oplus] (eccentric). As a result, we exclude the Trojan companions near the L4 point more massive than $\simeq 14 (15)$ [M_\oplus] if the orbit is circular, and $\simeq 74 (65)$ [M_\oplus] if the orbit is allowed to be eccentric, both at the 3σ level. Our constraint under the reasonable assumption of a circular orbit is more stringent than that of Ford & Gaudi (2006) by a factor of 4, because we have increased the number of radial velocity samples and because our data cover the critical phase to determine T_0 . Consequently, we conclude that we do not find any

⁸ Here M_T is defined as the difference in the mass at L4 ($M_{T,L4}$) and the mass at L5 ($M_{T,L5}$), namely $M_T \equiv M_{T,L4} - M_{T,L5}$.

sign of the existence of additional bodies in the TrES-1 system at present.

In this paper, we have placed a constraint on the sky-projected angle between the stellar spin axis and the planetary orbital axis for the TrES-1 system, namely $\lambda = 30 \pm 21$ [deg] using all available data and information from previous studies. Although we can not discriminate whether the spin-orbit angle in this system is well-aligned or not at this point, our constraint on λ clearly indicates the prograde orbital motion of TrES-1b. The uncertainty is larger than in previous studies (~ 1 [deg] for HD 209458 and HD 189733) because the host star is significantly fainter in this case. Although further radial velocity measurements during transit would be necessary to pin down λ more stringently, we have demonstrated for the first time that such measurements are possible for such a faint target. This is important because most of the newly discovered transiting planets from ongoing transit surveys will have relatively faint host stars. For example, the new targets that were discovered in 2006, namely XO-1 (McCullough et al. 2006), TrES-2 (O'Donovan et al. 2006), HAT-P-1 (Bakos et al. 2006), WASP-1 and WASP-2 (Cameron et al. 2007), are all in this category. Combining future measurements of λ in other transiting systems, we would be able to determine the distribution of λ for exoplanetary systems with useful statistical accuracy.

We acknowledge close support of our observations by Akito Tajitsu, who is a Support Scientist for Subaru HDS. We appreciate the detailed and helpful critique of the manuscript by the referee, Scott Gaudi. We also thank Kazuhiro Yahata, Shunsaku Horiuchi, Takahiro Nishimichi, and Hiroshi Ohmuro for useful discussions. N.N. is supported by a Japan Society for Promotion of Science (JSPS) Fellowships for Research. This work is supported in part by a Grant-in-Aid for Scientific Research from the JSPS (No.14102004, 16340053, 17740106), and MEXT Japan, Grant-in-Aid for Scientific Research on Priority Areas, "Development of Extra-solar Planetary Science," and NASA grant NAG5-13148. We wish to recognize and acknowledge the very significant cultural role and reverence that the summit of Mauna Kea has always had within the indigenous Hawaiian community.

References

Alonso, R., et al. 2004, *ApJL*, 613, L153
 Bakos, G. A., et al. 2006, *astro-ph/0609369*
 Cameron, A. C., et al. 2007, *MNRAS*, 1491
 Charbonneau, D., et al. 2005, *ApJ*, 626, 523
 Charbonneau, D., Brown, T. M., Burrows, A., & Laughlin, G. 2007, in *Protostars and Planets*, ed. V. B. Reipurth, D. Jewitt, and K. Keil (Tucson: University of Arizona Press), 701
 Gaudi, B. S. & Winn, J. N. 2007, *ApJ*, 655, 550
 Gillon, M., Pont, F., Moutou, C., Bouchy, F., Courbin, F., Sohy, S., & Magain, P. 2006, *A&A*, 459, 249
 Giménez, A. 2006, *ApJ*, 650, 408
 Ford, E. B. & Gaudi, B. S. 2006, *ApJL*, 652, L137
 Johnson, J. A., et al. 2006, *ApJ*, 647, 600
 Kobayashi, Y., et al. 1998, in *Proc. SPIE Vol. 3352, Advanced Technology Optical/IR Telescopes VI*, ed. L. M. Stepp, 120
 Laughlin, G., Wolf, A., Vanmunster, T., Bodenheimer, P., Fischer, D., Marcy, G., Butler, P., & Vogt, S. 2005, *ApJ*, 621, 1072
 Marzari, F., & Weidenschilling, S. J. 2002, *Icarus*, 156, 570
 McCullough, P. R., et al. 2006, *ApJ*, 648, 1228
 McLaughlin, D. B. 1924, *ApJ*, 60, 22
 Minezaki, T., Yoshii, Y., Kobayashi, Y., Enya, K., Suganuma, M., Tomita, H., Aoki, T., & Peterson, B. A. 2004, *ApJL*, 600, L35
 Narita, N., et al. 2005, *PASJ*, 57, 471
 Noguchi, K., et al. 2002, *PASJ*, 54, 855
 O'Donovan, F. T., et al. 2006, *ApJL*, 651, L61
 Ohta, Y., Taruya, A., & Suto, Y. 2005, *ApJ*, 622, 1118
 Ohta, Y., Taruya, A., & Suto, Y. 2006, *astro-ph/0611466*
 Pont, F., Zucker, S., & Queloz, D. 2006, *MNRAS*, 373, 231
 Press, W. H., Teukolsky, S. A., Vetterling, W. T., & Flannery, B. P. 1992, *Numerical recipes in C. The art of scientific computing* (Cambridge: University Press, —c1992, 2nd ed.)
 Queloz, D., Eggenberger, A., Mayor, M., Perrier, C., Beuzit, J. L., Naef, D., Sivan, J. P., & Udry, S. 2000, *A&A*, 359, L13
 Rasio, F. A. & Ford, E. B. 1996, *Science*, 274, 954
 Rossiter, R. A. 1924, *ApJ*, 60, 15
 Sato, B., Kambe, E., Takeda, Y., Izumiura, H., & Ando, H. 2002, *PASJ*, 54, 873
 Steffen, J. H. & Agol, E. 2005, *MNRAS*, 364, L96
 Weidenschilling, S. J. & Marzari, F. 1996, *Nature*, 384, 619
 Winn, J. N., et al. 2006a, *astro-ph/0612224*
 Winn, J. N., Holman, M. J., & Roussanova, A. 2006b, *astro-ph/0611404*
 Winn, J. N., et al. 2006c, *ApJL*, 653, L69
 Winn, J. N., et al. 2005, *ApJ*, 631, 1215
 Winn, J. N., Suto, Y., Turner, E. L., Narita, N., Frye, B. L., Aoki, W., Sato, B., & Yamada, T. 2004, *PASJ*, 56, 655
 Wu, Y. & Murray, N. 2003, *ApJ*, 589, 605
 Yoshii, Y. 2002, in *New Trends in Theoretical and Observational Cosmology*, ed. K. Sato & T. Shiromizu (Tokyo: Universal Academy Press), 235
 Yoshii, Y., Kobayashi, Y., & Minezaki, T. 2003, in *Bulletin of the American Astronomical Society*, 752

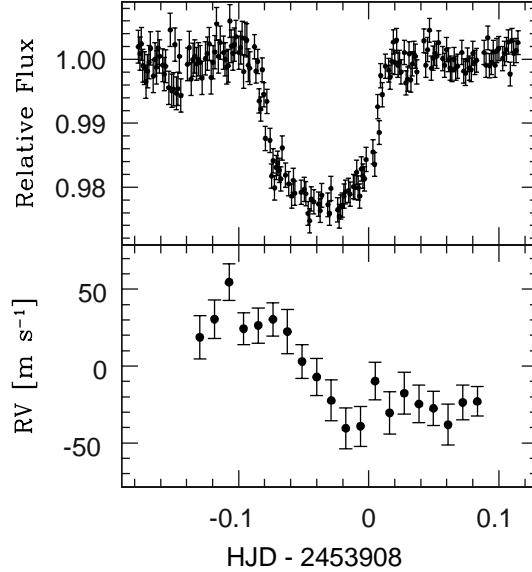


Fig. 1. Top: A photometric light curve from the MAGNUM observation (184 samples). The error-bars are scaled to satisfy $\chi^2/\nu_{dof} = 1.0$ (see Section 2.1.). Bottom: 20 radial velocity samples computed from the Subaru/HDS spectra. The values and uncertainties are presented in Table 1.

Table 1. Radial velocities obtained with the Subaru/HDS.

Time [HJD]	Value [m s ⁻¹]	Error [m s ⁻¹]
2453907.87018	18.7	14.0
2453907.88139	30.5	12.5
2453907.89262	54.6 ^a	12.0
2453907.90384	24.3	10.4
2453907.91506	26.4	11.4
2453907.92628	30.4	10.9
2453907.93750	22.4	14.3
2453907.94873	2.9	11.0
2453907.95996	-7.1	12.1
2453907.97119	-22.3	13.3
2453907.98241	-40.5	13.3
2453907.99364	-39.2	13.0
2453908.00488	-9.8	12.2
2453908.01610	-30.5	13.8
2453908.02732	-17.7	13.6
2453908.03854	-24.7	12.2
2453908.04978	-27.5	11.1
2453908.06100	-38.2	13.3
2453908.07223	-23.7	11.2
2453908.08345	-23.0	9.6

^a: A possible outlier.

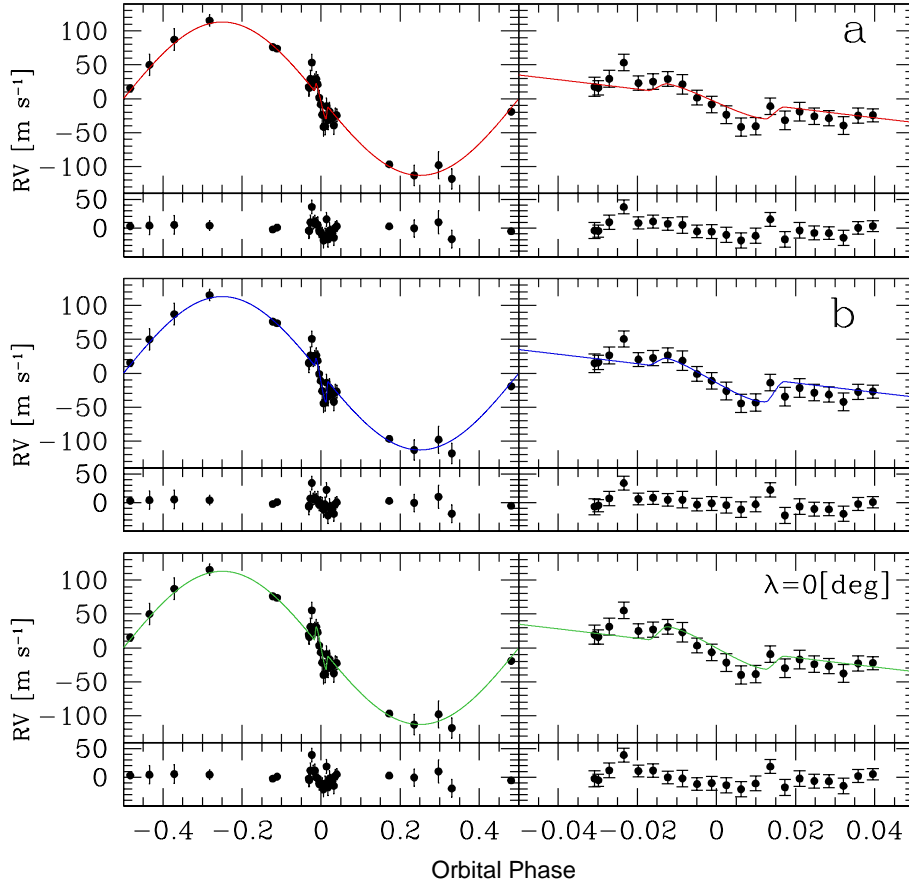


Fig. 2. Orbital plots of TrES-1 radial velocities and the best-fitting models, phased by $P = 3.0300737$ and $T_c(0) = 2453186.80603$. Top (marked with “a”): With the *a priori* constraint on $V \sin I_s$ (see text). Middle (marked with “b”): Without the constraint. Bottom (marked with “ $\lambda = 0$ [deg]”): Without the constraint and assuming that $\lambda = 0$ [deg]. Left panel: A radial velocity plot for the whole orbital phase. Right panel: A close-up of the radial velocity plot around the transit phase. The waveform around the central transit time is caused by the RM effect. Bottom panels: Residuals from the best-fit curve.

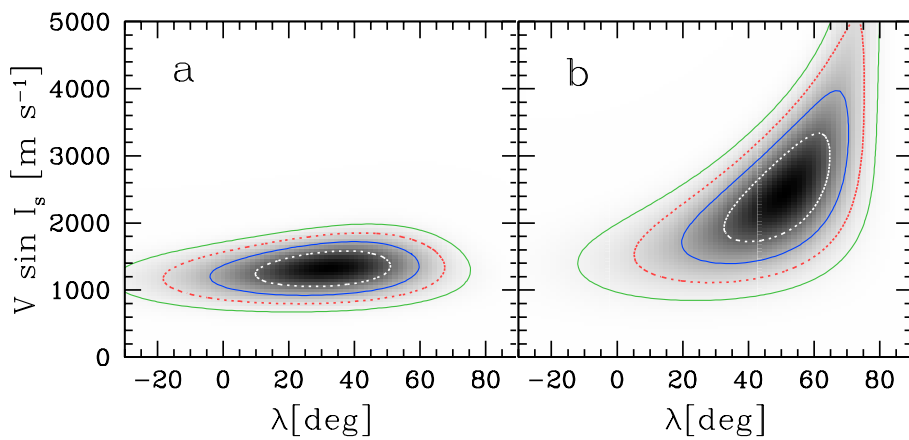


Fig. 3. Contours of constant χ^2 in $(V \sin I_s, \lambda)$ space, based on simultaneous fitting of 32 radial velocity samples and 1333 photometric samples, with (left, marked with a) and without (right, marked with b) the *a priori* constraint on $V \sin I_s$. The solid line represents $\Delta\chi^2 = 2.30$ (inner) and $\Delta\chi^2 = 6.17$ (outer), while the dotted line shows $\Delta\chi^2 = 1.00$ (inner) and $\Delta\chi^2 = 4.00$ (outer), respectively.

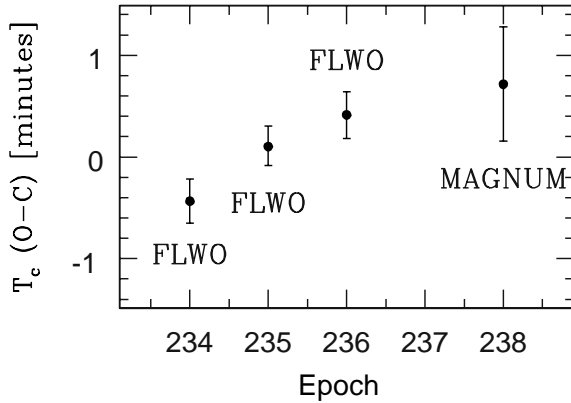


Fig. 4. Timing residuals of the time of mid-transit for each epoch (E), based on the ephemeris of Winn et al. (2006b). The results for $E = 234, 235, 236$ are determined by the FLWO photometry, while $E = 238$ is computed by the MAGNUM data.

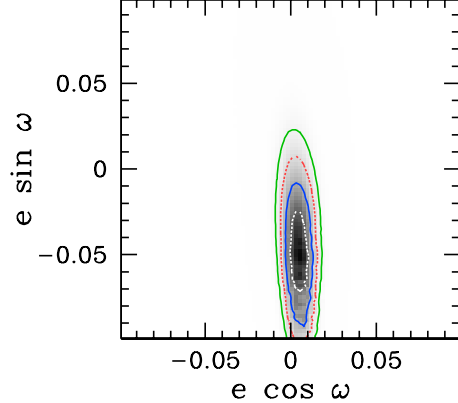


Fig. 5. Contours of constant χ^2 in $(e \cos \omega, e \sin \omega)$ space, based on simultaneous fitting of 32 radial velocity samples and 1333 photometric samples. At each grid point, all of the parameters except for (e, ω) were optimized. Contour line types are the same as those in Fig. 3

Table 2. Best-fit values and uncertainties^a of the free parameters.

Parameter	All data With the constraint		All data Without the constraint		Subaru/MAGNUM With the constraint	
	Value	Uncertainty	Value	Uncertainty	Value	Uncertainty
(All rv samples)						
K [m s $^{-1}$]	113.1	± 2.5	113.1	± 2.5	115.2 ^b	fixed
$V \sin I_s$ [km s $^{-1}$]	1.3	± 0.3	2.5	± 0.8	1.3	± 0.3
λ [deg]	30	± 21	48	± 17	28	± 24
u_V	0.57	± 0.05	0.57	± 0.05	0.59	± 0.05
u_z	0.37	± 0.03	0.37	± 0.03	–	–
R_p/R_s	0.1382	± 0.006	0.1382	± 0.006	0.13686 ^c	fixed
R_s [R_\odot]	0.82	± 0.02	0.82	± 0.02	0.811 ^c	fixed
i [deg]	88.4	± 0.3	88.4	± 0.4	88.9 ^c	fixed
v_1 [m s $^{-1}$]	1.3	± 3.0	4.0	± 3.5	0.7	± 2.9
v_2 [m s $^{-1}$]	–0.2	± 4.9	–0.2	± 4.9	–	–
v_3 [m s $^{-1}$]	–5.5	± 1.6	–5.5	± 1.6	–	–
$T_c(234) - 2453000$ [HJD]	895.84298	± 0.00015	895.84298	± 0.00015	–	–
$T_c(235) - 2453000$ [HJD]	898.87342	± 0.00014	898.87342	± 0.00014	–	–
$T_c(236) - 2453000$ [HJD]	901.90371	± 0.00016	901.90371	± 0.00016	–	–
$T_c(238) - 2453000$ [HJD]	907.96407	± 0.00034	907.96407	± 0.00034	907.96408	± 0.00034
(Without the outlier)						
K [m s $^{-1}$]	112.8	± 2.5	112.8	± 2.5	115.2 ^b	fixed
$V \sin I_s$ [km s $^{-1}$]	1.3	± 0.3	2.1	± 0.8	1.3	± 0.3
λ [deg]	24	± 23	39	± 21	22	± 27
v_1 [m s $^{-1}$]	1.1	± 3.1	0.9	± 3.6	–1.5	± 3.0

^a:Computed by $\Delta\chi^2 = 1.00$. ^b:Alonso et al. (2004). ^c:Winn et al. (2006b).